Association between Shape of Sclera and Myopic Retinochoroidal Lesions in Patients with Pathologic Myopia

Kyoko Ohno-Matsui,[1] *Masahiro Akiba,*[2] *Toshio Modegi,*[3] *Makoto Tomita,*[4] *Tatsuro Ishibashi,*[5] *Takashi Tokoro,*[1] *and Muka Moriyama*[1]

Purpose. The purpose of the study was to analyze the shape of the sclera determined by swept-source optical coherence tomography (OCT) and to determine the relationship between the shape and the myopic retinochoroidal lesions.

Methods. We studied 488 eyes of 272 patients with high myopia (refractive error ≥−8.00 diopters [D] or axial length >26.5 mm) and 43 emmetropic eyes of 43 controls (refractive error ≤±3 D). An image of the sclera was obtained by a swept-source OCT prototype instrument that uses a wavelength sweeping laser centered on 1 μm wavelength with an A-scan repetition rate of 100,000 Hz. The scans were 12 mm radial scans centered on the fovea. Seventy eyes were also examined by three-dimensional magnetic resonance imaging (3D MRI) to obtain the contour of the outer surface of the eyes. The main outcome measures, visibility of the entire sclera layer, scleral thickness, scleral contour, and location of the most protruded point of the globe, were obtained by swept-source OCT and 3D MRI.

Results. The entire thickness of the sclera was observed in 278 of 488 (57.0%) highly myopic eyes, but the outer border was not observed in any of the emmetropic eyes. The mean subfoveal scleral thickness was 227.9 ± 82.0 μm in the highly myopic eyes. The sclera was thickest at 3000 μm nasal to the fovea. The curvatures of the inner scleral surface of highly myopic eyes could be divided into curvatures that sloped toward the optic nerve, those that were symmetrical and centered on the fovea, those that were asymmetrical, and those that were irregular. Patients with irregular curvature were significantly older and had significantly longer axial lengths than those with other curvatures. Myopic fundus lesions were present significantly more frequently in the eyes with irregular curvature. All of the eyes whose scleral curvature sloped toward the optic nerve had nasally distorted shape in the 3D MRI images, and all eyes with temporally dislocated shape had irregular curvature.

Conclusions. In vivo evaluations of the sclera in highly myopic eyes by swept-source OCT can provide important information on deformations of the sclera and how such deformities are related to myopic fundus lesions. (*Invest Ophthalmol Vis Sci.* 2012;53:6046–6061) DOI:10.1167/iovs.12-10161

Pathologic myopia is a major cause of visual impairments worldwide.[1–6] The visual impairments are mainly caused by different types of myopic lesions in the retina and choroid, especially in the macula and optic disc areas.[7–10] However, what causes the development of these myopic lesions has not been determined, and the lack of this information has made it difficult to design therapy to reduce or prevent the development of these lesions.

To try to determine the mechanism that causes the development of myopic lesions, we analyzed the shape of the external surface of highly myopic eyes by high-resolution three-dimensional magnetic resonance imaging (3D MRI). We found that highly myopic eyes were not simply elongated but had out-pouched areas especially in the posterior pole of the eye.[11] We also found that the visual field defects[7] that were not due to a myopic fundus lesions were present significantly more frequently in eyes with temporally distorted shapes than in eyes with distortions in other areas.[11] In another study on highly myopic eyes, we found that visual field defects were observed significantly more frequently in eyes with type IX staphyloma (classification by Curtin[12]), which is the type with a ridge-like protrusion temporal to the optic disc. These findings suggested that eye shapes and deformities, especially in the posterior segment of the eye, are most likely related to the development of the myopic lesions.

We thus asked whether the shape of the sclera also was significantly associated with myopic fundus lesions. The sclera forms the principal part of the outer coat of the eye, and it helps maintain a stable ocular dimension and protects the intraocular structures. The properties of the sclera are critical in determining the size and shape of the eye.[13] The sclera consists mainly of type I collagen and is relatively avascular.[13] A histological study showed that highly myopic eyes had thinner sclera particularly at the posterior pole,[14] and the thinning was associated with a narrowing and dissociation of the collagen fiber bundles and a reduction in collagen fibril diameter.[9,14,15] Highly myopic eyes also have differences in the biochemical makeup of the sclera, such as alterations of the glycosaminoglycan and collagen content.[16] Unfortunately, these findings were made in postmortem human eyes,[17] although sclera thinning has also been observed in animal models of experimental myopia.[18–20]

From the [1]Department of Ophthalmology and Visual Science and the [4]Clinical Research Center, Tokyo Medical and Dental University, Tokyo, Japan; [2]Topcon Corporation, Tokyo, Japan; [3]Dai Nippon Printing Co., Ltd., Tokyo, Japan; and the [5]Department of Ophthalmology, Kyushu University, Fukuoka, Japan.

Supported in part by research Grants 22390322 and 23659808 from the Japan Society for the Promotion of Science, Tokyo, Japan.

Submitted for publication May 7, 2012; revised June 19 and July 17, 2012; accepted July 28, 2012.

Disclosure: **K. Ohno-Matsui**, None; **M. Akiba**, Topcon Corporation (E); **T. Modegi**, None; **M. Tomita**, None; **T. Ishibashi**, None; **T. Tokoro**, None; **M. Moriyama**, None

Corresponding author: Kyoko Ohno-Matsui, Department of Ophthalmology and Visual Science, Tokyo Medical and Dental University; 1-5-45 Yushima, Bunkyo-ku, Tokyo 113-8510, Japan; k.ohno.oph@tmd.ac.jp.

Investigative Ophthalmology & Visual Science, September 2012, Vol. 53, No. 10

In spite of the importance of the sclera in determining the size and shape of the eye, detailed information on the biometrics of the sclera is limited, and the information published has been mainly obtained from postmortem tissues. Thus, it is difficult to extend these findings to the eye in situ and to determine the relationship of these findings to the development of myopic lesions.

Recent advances in optical coherence tomography (OCT) have enabled investigators to image the tissues deeper than the neural retina such as choroid and sclera. A PubMed search identified only two articles reporting on the appearance of the sclera in the macular area obtained by OCT.[21,22] In one paper, Imamura et al.[21] reported the use of enhanced-depth imaging OCT (EDI-OCT), and showed that the subfoveal sclera was significantly thicker in highly myopic eyes with a dome-shaped macula (DSM), a protrusion of the macula within a staphyloma,[23] than in highly myopic eyes without a DSM. Maruko et al.[22] measured scleral thickness in the posterior fundus in the images obtained by a prototype swept-source OCT in nine patients with the tilted-disc syndrome (TDS) with a mean axial length of 24.89 ± 1.05 mm. They reported that the subfoveal sclera was significantly thicker than the sclera superior and inferior to the fovea. Both of these studies showed that in vivo observations of the sclera of human eyes can be made by OCT.

Swept-source OCT is a relatively new instrument that uses a wavelength-sweeping laser as the light source[24] and has less sensitivity roll-off with tissue depth than conventional spectral-domain OCTs. The current swept-source OCT instruments use a longer central wavelength, generally in the 1 μm range, which has improved their ability to penetrate deeper into tissues than the conventional spectral-domain OCT instruments. With this deeper penetration, evaluations of the choroid and sclera are potentially possible.

Because we are interested in determining the mechanism causing myopic fundus lesions, we have been examining the morphology of the deeper tissues in the macular and peripapillary regions of highly myopic eyes in patients in our High Myopia Clinic by swept-source OCT.[25–28] We argue that swept-source OCT will provide more detailed images of the choroid and sclera even though the scanned area is smaller and more limited than with MRI. Swept-source OCT has the advantage of enabling the user to analyze the spatial relationship between the morphology of the retina/choroid and the myopic fundus lesions because it can show different eye structures in the same scan. We expected that this information would provide clues to how such deformities can lead to vision-threatening lesions specific to pathologic myopia.

Thus, the purpose of this study was to analyze the morphological features of the sclera in the posterior pole and to analyze the scleral contour in a large number of highly myopic eyes by swept-source OCT. We showed that the entire layer of the sclera was clearly visible in 57% of the highly myopic eyes and that the contour of the sclera can be divided into four distinct patterns. Examinations of the four patterns showed that some were significantly associated with myopic lesions. We also compared the shape of the eye obtained by swept-source OCT to that obtained by 3D MRI. These results showed not only that the shape of highly myopic eyes is distorted but also that the distortions are related to the development of vision-threatening complications in patients with pathologic myopia.

Methods

The procedures used in this research adhered to the tenets of the Declaration of Helsinki and were approved by the Ethics Committee of Tokyo Medical and Dental University. A written informed consent was obtained from all participants for the original examination procedures.

Two hundred seventy-two consecutive patients with pathologic myopia were evaluated by swept-source OCT from May 6, 2011, to December 9, 2011, in the High Myopia Clinic at Tokyo Medical and Dental University, Tokyo. The definition of pathologic myopia was a refractive error (spherical equivalent) >-8.00 diopters (D) or an axial length >26.5 mm. Forty-three eyes of 43 subjects with refractive errors $\leq\pm 3$ D were classified as emmetropic and were examined in the same way. All of the emmetropic participants were current or former staff members of our university and all volunteered. Patients whose swept-source OCT images were of poor quality due to a dense cataract, poor fixation because of macular chorioretinal atrophy, or myopic macular holes were excluded. Patients with a history of vitreoretinal surgery were also excluded because such surgery could affect the scleral contour.

All of the participants had a comprehensive ocular examination including measurements of the refractive error (spherical equivalent), axial length with the IOLMaster (Carl Zeiss Meditec, Dublin, CA), and fundus biomicroscopy. The presence of a posterior staphyloma was determined by stereoscopic fundus examinations.

Swept-Source OCT

All the eyes were examined by a prototype swept-source OCT instrument manufactured by Topcon Corporation (Tokyo, Japan). This OCT system has an A-scan repetition rate of 100,000 Hz, and its light source is a wavelength-sweeping laser centered at 1050 nm with an approximate 100 nm bandwidth, although the effective bandwidth was approximately 60 nm because of water absorption. The axial resolution was calculated to be 8 μm in tissue with a lateral resolution of 20 μm. The imaging depth was 2.6 mm in tissue, and the lateral scan length was adjustable. For our scanning protocol, 12 mm scans along 12 meridians centered on the fovea were performed. A single image was made up of 1024 A-line scans acquired in 10 ms. Typically, 32 B-scan images were recorded and averaged by postprocessing to yield a despeckled high-quality B-scan image.

The central retinal thickness was measured with the caliper function of the built-in software of the OCT. The scleral thickness was measured at the fovea and at four different areas: 3 mm superiorly, inferiorly, temporally, and nasally to the fovea. These measurements were made by one masked author (MM). Because the choroid was too thin to be measured in many highly myopic eyes, the number of eyes whose choroid was too thin to be measured was counted instead.

The contour of inner scleral surface, the chorioretinal interface, was outlined manually in each eye, and the eyes were classified according to their contour. In some eyes with pathologic myopia, the peak of the curvature of the posterior segment did not correspond to the center of the fovea. In these eyes, the most posteriorly protruded point in the fundus was identified. The most protruded part was identified in each of 12 radial scans centered on the central fovea, and the depth of the most protruded part from the foveal plane was measured in each scan (Fig. 1A). Then the scan that included the most protruded part was determined. The distance of the most protruded point from the fovea as well as the depth of the most protruded point from the foveal plane was measured with the caliper function of the built-in software of the OCT by one masked author (MM). For the distribution of the most protruded point, we combined the superior, superior–temporal, and superior–nasal findings and called this segment the upper quadrant, and we also combined the lower, temporal–lower, and nasal–lower findings and called this segment the lower quadrant (Fig. 1B).

Analysis of Eye Shape by High-Resolution 3D MRI

We recently reported that it was possible to obtain a complete topographic image of human eyes by high-resolution 3D MRI.[11] We compared the contour of the inner scleral surface seen in the OCT

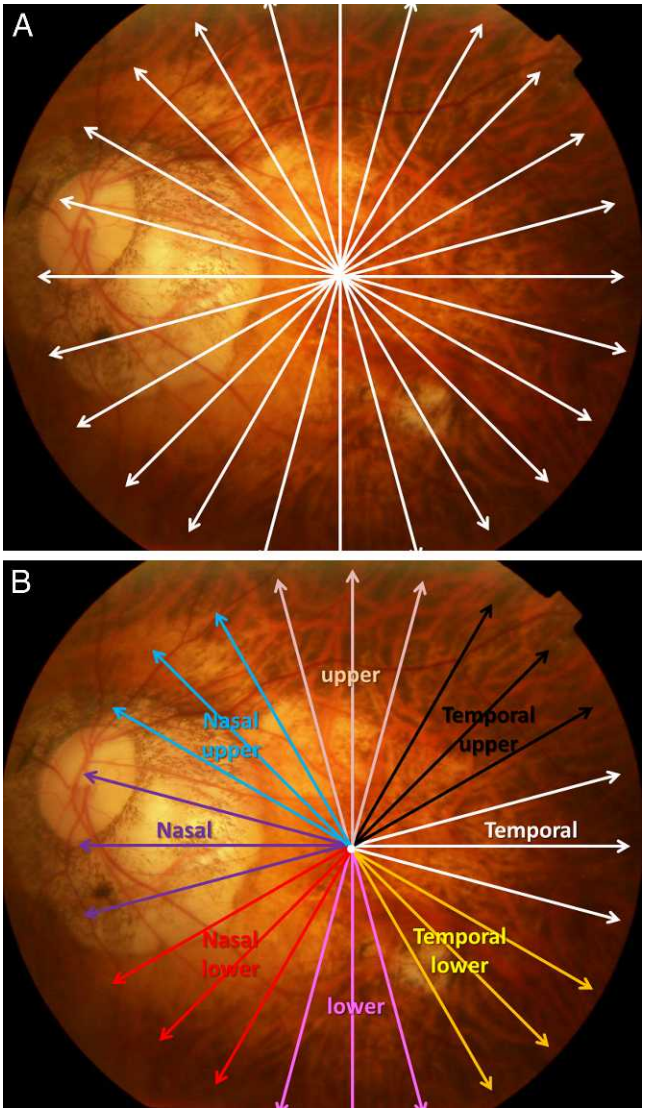

Figure 1. Area scanned by swept-source OCT superimposed on fundus photograph. (**A**) Area scanned by 12 mm meridian scans centered on the central fovea. The angle between each pair of scans is 15°. (**B**) Classification of the 12 meridian scans into eight categories according to their orientations.

images and the shape of the outer surface of the eye obtained by 3D MRI. We have developed software to analyze the human eye shape obtained by 3D MRI, and we used this software to automatically analyze the degree of symmetry of the posterior eye segment in the horizontal and sagittal planes. We also determined the pointedness or bluntness of the posterior pole of the eye (Fig. 2). Briefly, the view of the eyes from six points, namely the front, back, superior, inferior, nasal, and temporal, was incorporated into the software of the 3D MRI. Then, a central axis line passing through the geometric center of the eye was automatically drawn. The point of intersection of the central axis and the posterior margin of the eye was defined as the basal point (P_b). Then, a point on the central axis 87 pixels, approximately 12.5 mm, anterior to the P_b was defined as the point of origin (P_o) of the measurements; the purpose was to avoid the influence of axial length on the location of P_o.

Next, P_o was rotated 22.5° nasally in the horizontal plane, and a line was drawn posteriorly. Where the line intersected the margin of the eye was called P_n. Similarly, P_o was rotated 22.5° temporally in the horizontal plane, and where the line from P_o intersected the margin of the eye was called P_t. In the sagittal plane, P_o was rotated either inferiorly or superiorly, and where lines intersected margin of the eye was called P_i or P_s, respectively. The area of the segment formed by P_o, P_b, and P_n was defined as S_n; the area of the segment formed by P_o, P_b, and P_t was defined as S_t; the area formed by P_o, P_b, and P_i was defined as S_i; and the area formed by P_o, P_b, and P_s was defined as S_s. The degree of symmetry in the horizontal plane was expressed by the ratio of S_n and S_t, and the degree of symmetry in the sagittal plane was expressed by the ratio of S_i and S_s. The posterior surfaces with ratios between 90 and 110 were classified as symmetrical.

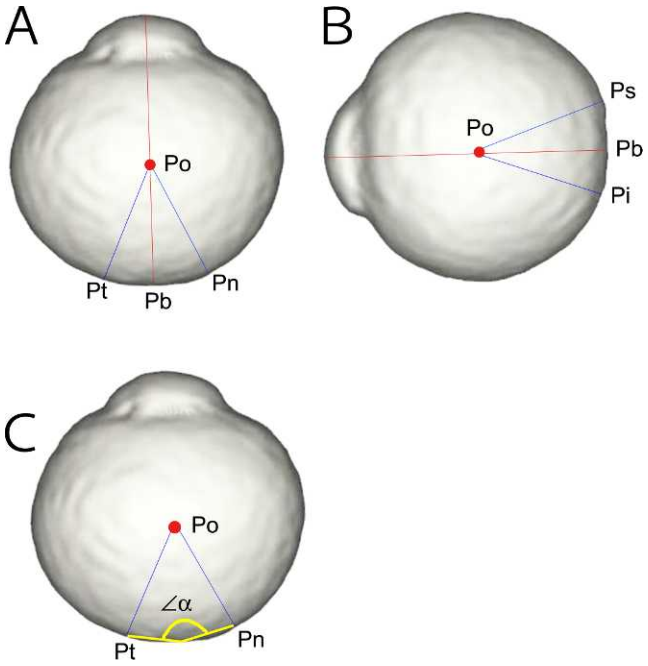

Figure 2. Degree of symmetry and pointedness of the posterior segment of the eye obtained by 3D MRI. (**A**) Inferior view from which the horizontal symmetry was determined. The point of intersection between the central axis and the posterior edge of the eye was defined as the basal point (P_b). Then, the point on the central axis 87 pixels away from P_b was defined as the measurement point of origin (P_o). Next, the point that was rotated 22.5° nasally (P_n) or temporally (P_t) was determined. The area of the arc surrounded by P_o, P_b, and P_n was defined as S_n; the area of the arc surrounded by P_o, P_b, and P_t was defined as S_t; the area of the arc surrounded by P_o, P_b, and P_i was defined as S_i; and the area of the arc surrounded by P_o, P_b, and P_s was defined as S_s. The horizontal symmetry is given by the ratio of S_n and S_t. (**B**) The sagittal symmetry was determined by the nasal view of the 3D MRI image. P_b and P_o were determined as described for (**A**). The point that was rotated 22.5° superiorly (P_s) or inferiorly (P_i) was determined. The area of the arc surrounded by P_o, P_b, and P_i was defined as S_i, and the area of the arc surrounded by P_o, P_b, and P_s was defined as S_s. The sagittal symmetry is given by the ratio of S_i and S_s. (**C**) The angle $<P_n$–P_b–P_t was defined as the posterior sharpness.

For the sharpness of the posterior surface, the angle formed by P_n, P_b, and P_t was defined as the posterior sharpness angle. The shape of the posterior segments of the globe was defined as "pointed" when this angle was $\leq$150°, and the shape of posterior segment of the eye was defined as "dull" when this angle was >150°.

Statistical Analyses

The patients' age, refractive error, axial length, central retinal thickness, and scleral thickness were compared between eyes whose entire scleral layer was visible and those whose entire scleral layer was not visible in the OCT images by Welch's *t*-tests and Student's *t*-tests. The number of eyes whose choroid was too thin to be measured and the prevalence of a posterior staphyloma were compared between

Table 1. Demographics of Patients with Pathologic Myopia

Sex, No. of eyes (No. of persons)	
Men	131 (75)
Women	357 (197)
Age, y, mean ± SD	57.1 ± 13.8 (12–89)
Refractive error, d, mean ± SD	−13.3 ± 4.1 (−8.5 to −25.5)
Axial length, mm, mean ± SD	29.9 ± 2.0 (26.6–36.6)
Posterior staphyloma, No. of eyes (%)	
Present	412 (84.4%)
Absent	76 (15.6%)

groups using Fisher's exact probability tests or χ^2 tests. The clinical characteristics of eyes with the four distinct patterns of curvature of the posterior fundus were analyzed using one-factor analysis of variance (ANOVA). The correlation between the subfoveal scleral thickness and the patient's age and axial length was analyzed using Pearson tests for rank correlation coefficients. For bilaterally affected eyes, one eye was randomly selected using random number tables for statistical analyses. A P value < 0.05 was considered statistically significant.

Results

Five hundred forty-four eyes of 272 consecutive patients were examined in our High Myopia Clinic, and these patients also underwent swept-source OCT. Of these 544 eyes, 56 eyes were excluded because of poor fixation during the OCT examination due to large macular atrophy (35 eyes), low-quality OCT images due to dense cataracts (5 eyes), or history of vitreoretinal surgery (6 eyes). The remaining 10 eyes were excluded because these eyes were not highly myopic in these patients with unilateral high myopia. In the end, 488 eyes of 272 highly myopic patients were studied; their demographics are shown in Table 1. A posterior staphyloma was present in 412 eyes (84.4%) and was absent in 76 eyes (15.6%).

Swept-Source OCT Findings for Sclera in Eyes with Pathologic Myopia

The sclera was observed as a relatively uniform hyperreflective structure exterior to the thin choroid in the swept-source OCT images (Fig. 3). We were also able to observe the retrobulbar orbital fat beyond the sclera in eyes with pathological myopia. A close observation of the deeper tissues showed a relatively hyporeflective layer outlining the sclera (Fig. 3). This hyporeflective layer was in close contact with the outer surface of the sclera and appeared to break up into smaller bundles and blend into the orbital fat tissue posteriorly (Figs. 3E, 3F). The hyporeflective layer was considered to be the episclera and Tenon's capsule.[13] In some scans, cross sections of episcleral blood vessels were observed posterior to the sclera (Fig. 3E).

Factors Significantly Correlated with Visibility of Entire Sclera

To be able to measure the sclera thickness, it was necessary to determine whether the entire sclera was visible in the swept-source OCT images. Our findings showed that the entire scleral layer was observed in all 12 radial scans in 278 of 488 eyes (57.0%) and not observed in any of the 12 radial scans in 180 of 488 eyes (36.9%). A DSM, a convex elevation of the macula that differed from a surrounding staphyloma,[21,23] was observed in 93 of 488 eyes. In 32 of these 93 eyes, the entire scleral layer was visible in all 12 radial scans; in the other 31 eyes, the outer border of the sclera was visible in none of the scans. In the remaining 30 eyes, the sclera in the macular area was too thick to allow a view of the outer border of the sclera due to the DSM, although the entire scleral layer was visible in areas outside the DSM area.

The clinical characteristics of the 278 eyes of 175 patients whose entire scleral layer was visible in all 12 radial scans, as well as those of the 180 eyes of 114 patients whose outer scleral border was not visible in any of the 12 radial scans, are shown in Table 2. In 17 patients, the entire scleral layer was visible in one eye but not visible in the fellow eye. The patients whose entire scleral layer was visible were significantly older, were significantly more myopic, and had significantly longer axial lengths than those whose entire scleral layer was not visible (Table 2).

A posterior staphyloma was present in all 278 eyes whose entire scleral layer was visible, whereas a staphyloma was found in 57.8% of the 180 eyes whose entire scleral layer was not visible ($P < 0.05$, Fisher's exact probability tests).

Sixty-five of 278 eyes whose entire scleral layer was visible were excluded from the central retinal thickness measurements: 44 eyes due to macular retinoschisis, 2 eyes due to macular holes, 4 eyes due to macular atrophy, and 15 eyes due to myopic choroidal neovascularization (CNV). Similarly, 15 of 180 eyes whose entire scleral layer was not visible were excluded from the measurements of central retinal thickness: 8 eyes due to macular retinoschisis, 1 eye due to macular atrophy, and 6 eyes due to myopic CNV. In the end, the central retinal thickness was compared between 213 of 278 eyes whose entire scleral layer was visible and 165 of 180 eyes whose entire scleral layer was not visible.

The results showed that the central retina in the eyes whose entire scleral layer was visible was significantly thinner than in those whose entire scleral layer was not visible (Table 2). There was a significant negative correlation between central retinal thickness and axial length ($r = -0.19$, $P = 0.0007$, Pearson's correlation coefficient test), while the correlation was not significant between central retinal thickness and the age of the patient.

In many eyes with pathologic myopia, the subfoveal choroidal thickness was too thin to measure. Thus, we counted the number of eyes whose subfoveal choroid was too thin and compared the frequencies between the eyes where the entire sclera layer was visible and those in which the entire sclera layer was not visible. This measurement was made by one masked author (MM). The subfoveal choroid was too thin to be measured in 239 of 278 eyes (86.0%) whose entire layer of sclera was visible; this was the case significantly more frequently than in the eyes whose entire scleral layer was not visible (29 of 151 eyes [16.1%]) ($P = 1.5 \times 10^{-48}$, χ^2 tests).

Scleral Thickness in Different Regions of Posterior Pole in Highly Myopic Eyes

We measured the scleral thickness in different regions of highly myopic eyes whose entire scleral layer was visible in all 12 meridians in the OCT images. We excluded 32 of 278 eyes with a DSM. Thus, 246 eyes were analyzed, and the mean subfoveal scleral thickness was 227.9 ± 82.0 μm, with a range of 80 to 546 μm in these eyes. The subfoveal scleral thickness was significantly correlated with the axial length ($r = -0.35$, $P = 2.8 \times 10^{-7}$, Pearson tests for rank correlation coefficients), but the subfoveal scleral thickness was not significantly correlated with the age of the patient.

Scleral thickness was also measured in the 246 eyes at 3 mm temporal, superior, and inferior to the fovea. The scleral thickness was not measured at 3 mm nasal to the central fovea in 29 eyes because of the presence of a scleral ridge temporal

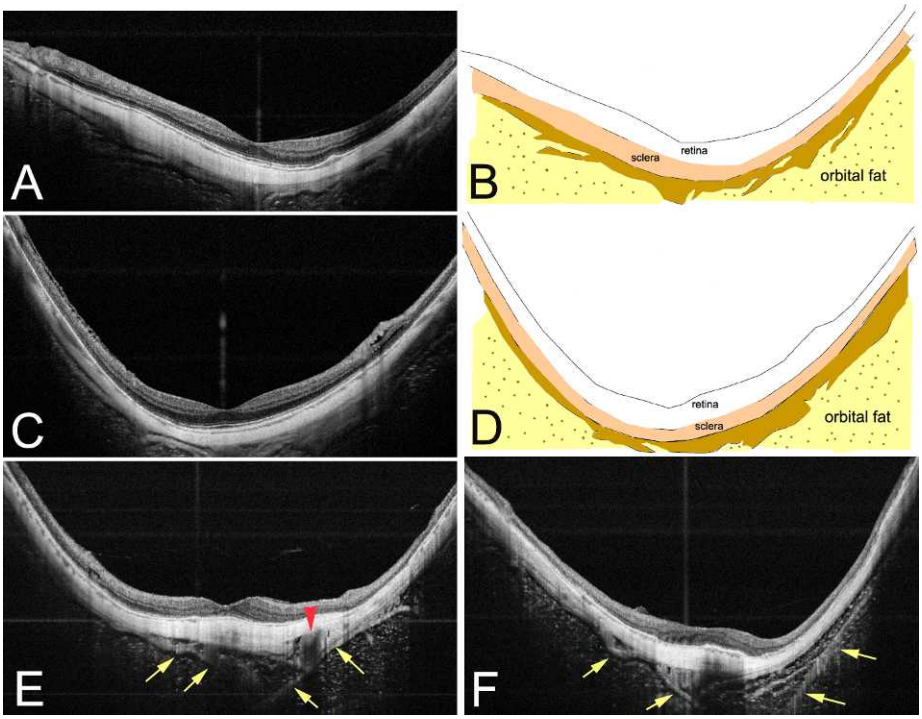

Figure 3. Observations of the sclera and Tenon's capsule in highly myopic eyes by swept-source OCT. (**A**, **C**) The sclera is observed as the highly reflective tissue outside the very thin choroid. A less reflective tissue can be seen outside the sclera. Orbital fat tissue is also observed as grayish tissue with many dots. (**B**, **D**) Schematic drawings of (**A**) and (**C**), respectively, with the tissues labeled. The sclera is colored *orange* and the tissue outside the sclera, suggestive of Tenon's capsule and episclera, is colored *brown*. (**E**, **F**) The fibers (*arrows*) of Tenon's capsule appear to spread and blend into the orbital fat tissue posteriorly. Cross sections of episcleral blood vessels can be seen posterior to the sclera (*arrowhead*, **E**).

to the optic disc due to type IX staphyloma.[12,29] The mean scleral thickness was 190.7 ± 71.6 μm with a range of 65 to 488 μm at 3 mm superior to the central fovea, 182.7 ± 70.2 μm with a range of 53 to 414 μm inferior, 181.8 ± 75.1 μm with a range of 45 to 453 μm temporal, and 252.8 ± 90.8 μm with a range of 74 to 513 μm nasal to the fovea. Statistical analyses showed that subfoveal scleral thickness was significantly greater than that at 3 mm temporal to the fovea, than that at 3 mm upper to the fovea, and than that at 3 mm lower to the fovea ($P < 0.001$, paired *t*-tests). The subfoveal scleral thickness was significantly less than that at 3 mm nasal to the fovea ($P < 0.001$, paired *t*-tests). In fact, the sclera at 3 mm nasal to the central fovea was significantly thicker than that at the subfoveal, temporal, superior, and inferior regions ($P < 0.001$, paired *t*-tests). The scleral thickness was not significantly different between the temporal area and the area superior to the fovea, between the temporal area and the area inferior to the fovea, or between the areas superior and inferior to the fovea.

When all these findings are combined, the sclera was thickest in the area nasal to the central fovea, followed by the subfoveal area, and then by the areas temporal, superior, and inferior to the fovea.

Four Different Types of Curvature of Inner Scleral Surface of Highly Myopic Eyes

In emmetropic eyes, the curvature of Bruch's membrane was not similar to the curvature of the inner scleral surface mainly because the choroid was thick and the choroidal thickness

Table 2. Comparison of Clinical Characteristics between Highly Myopic Eyes Whose Entire Scleral Layer was Visible and Those Whose Entire Scleral Layer was not Visible

	Visibility of the Outer Border of Sclera		
	Yes, in All 12 Radial Scans	**No, in None of the 12 Radial Scans**	***P* Value**
No. of eyes (No. of persons)	278 (175)	180 (114)	
Age, y, mean ± SD	60.9 ± 11.4 (32–89)	54.1 ± 16.4 (12–85)	0.0006*
Refractive error, d, mean ± SD	−15.1 ± 4.3 (−8.5 to −25.5)	−11.4 ± 3.0 (−8.5 to −18.5)	<0.0001†
Axial length, mm, mean ± SD	30.7 ± 1.9 (26.5–36.6)	28.2 ± 1.9 (26.5–32.5)	<0.0001†
Posterior staphyloma, No. of eyes (%)			
Present	278 (100%)	104 (57.8%)	<0.05‡
Absent	0 (0%)	76 (42.2%)	
Central retinal thickness, μm, mean ± SD	140.5 ± 35.4 (59–230)	158.5 ± 36.8 (52–253)	<0.0001†

* Welch's *t*-tests.
† Student's *t*-tests.
‡ Fisher's exact probability tests.

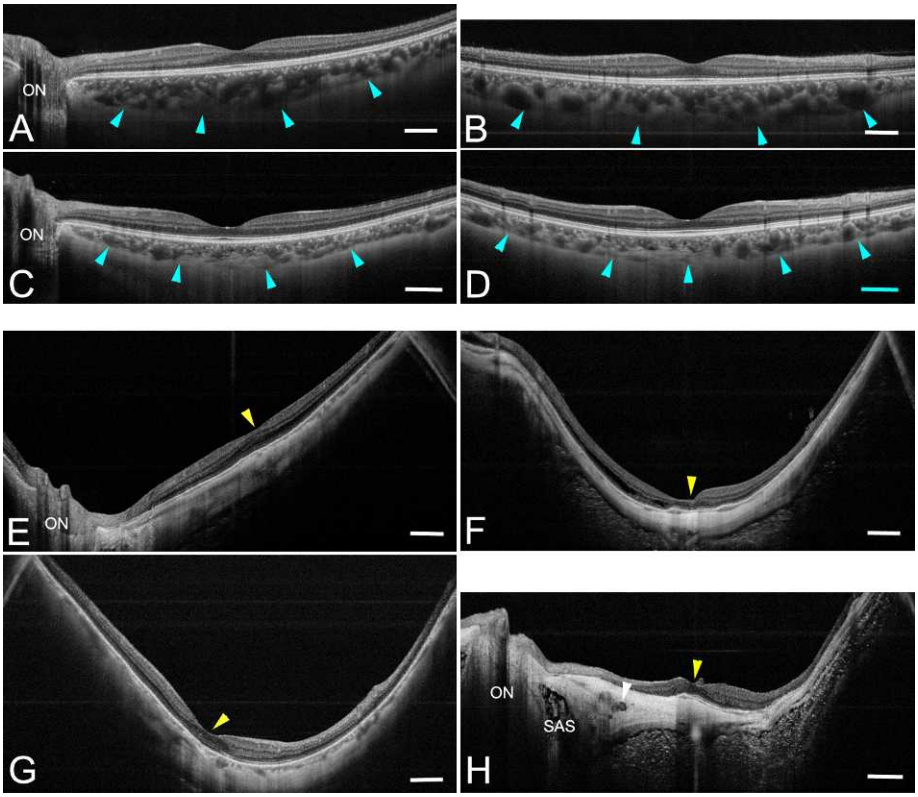

Figure 4. Different curvature patterns of the inner scleral surface. (**A–D**) Emmetropic eyes. In emmetropic eyes, the curve of inner scleral surface is not necessarily the same as the curve of the retinal pigmented epithelium (RPE) because a thick choroid exists between the RPE and sclera. (**A**) Horizontal scan through the central fovea shows that the RPE line is almost straight and is sloped toward the optic nerve. The curvature of the inner scleral surface (*arrowheads*) is slightly bowed and symmetric around the fovea. (**B**) Vertical scan through the central fovea of the same eye shown in (**A**) shows that the RPE line is almost straight. The curve of inner scleral surface (*arrowheads*) is slightly bowed and symmetrical around the fovea. (**C**) Horizontal scan through the central fovea shows that the RPE line is slightly bowed and the fovea is situated on the bottom of RPE curve. The curvature of the inner scleral surface (*arrowheads*) is slightly bowed and symmetrical around the fovea. (**D**) Vertical scan through the central fovea of the same eye shown in (**C**) shows that the RPE line is slightly bowed. The curvature of inner scleral surface (*arrowheads*) is slightly bowed and symmetric around the fovea. (**E–H**) Four distinct patterns of inner scleral curvature in highly myopic eyes. Due to a very thin choroid, the curvature of the inner scleral surface is almost identical to the RPE curvature, although the RPE can be atrophied in some cases. (**E**) The curvature is sloped toward the optic nerve. The curve of inner scleral surface is straight, and the optic disc is at the bottom of the posterior segment of the eye. This pattern was more obvious in horizontal than in vertical scans. The central fovea (*arrowhead*) is on the wall of the slope inclined toward the optic nerve. (**F**) The curvature is symmetrical around the fovea. The sclera is strongly bowed posteriorly; however, the curve is symmetrical around the fovea (*arrowhead*), and the fovea is situated on the bottom of posterior segment of the eye. (**G**) Asymmetrical curvature around the fovea. The sclera is strongly bowed posteriorly, and the most protruded point is away from the central fovea. The fovea (*arrowhead*) is on the slope. (**H**) Irregular curvature. The sclera is irregular and does not have a smooth curvature. The fovea is shown by the *yellow arrowhead*. Intrascleral artery is shown by *white arrowhead*. ON, optic nerve; SAS, subarachnoid space.

affected the scleral curvature. The curvature of the retinal pigment epithelium (RPE) and Bruch's membrane in emmetropic eyes had two patterns; the contour was straight and sloped toward the optic disc (Figs. 4A, 4B) or had a roughly symmetrical curvature centered on the fovea (Figs. 4C, 4D). Despite the different patterns of curvature of the RPE and Bruch's membrane, the curvature of the inner scleral surface was always symmetrical and mainly centered on the fovea.

Analysis of the contour of the inner scleral surface of 93 eyes of 75 patients with DSM and 28 eyes of 21 patients with TDS was not performed. We defined a TDS as a condition in which the upper part of the optic disc protruded anteriorly and the lower part of the optic disc sloped posteriorly in the stereoscopic fundus photographs.

In the end, the contour of the inner sclera of 367 of 488 highly myopic eyes was analyzed. The contour of the inner scleral surface had four distinct patterns (Figs. 4E–H; Table 3). The number of patients whose two eyes had different patterns was 45. The first pattern was one in which the curvature sloped toward the optic disc and the optic disc was at the bottom of the curvature (Fig. 4E). This pattern was observed in 44 of 367 eyes (12.0%) and was generally seen more clearly in horizontal than in vertical scans. In the second pattern, the curvature of the inner scleral surface was symmetrically centered on the fovea, and the fovea was situated in the center and at the bottom of the curvature (Fig. 4F). This pattern appeared to be similar to the second pattern seen in emmetropic eyes; however, the curvature appeared to be sharper than that in emmetropic controls. This type was observed in 98 of 367 eyes (26.7%). The third pattern was that in which the contour of the inner scleral surface was curved posteriorly with the curvature asymmetrical around the central fovea. The fovea was not situated at the bottom of the curvature but on the slope of the wall (Fig. 4G). This pattern was observed in 105 of 367 eyes (28.6%). The final pattern was the type in which the contour of the inner scleral surface was irregular and did not form a smooth circular arc (Figs. 4H, 5). In extreme cases, the curvature of the posterior eye segment was totally irregular (Fig. 5E). This was the most frequent pattern in eyes with pathologic myopia, one that we observed in 120 of 367 eyes (32.7%). The first pattern was significantly less frequently

observed than any other pattern ($P < 0.05$, χ^2 tests), but the differences in the incidences of the other three patterns were not significant.

Association of Clinical Characteristics of Highly Myopic Eyes with Different Types of Curvature of Posterior Segment of Eye

The clinical characteristics of highly myopic eyes with the four distinct patterns of curvature of the posterior fundus are shown in Table 3. Statistical analyses showed that the patients with irregular curvature were significantly older, significantly more myopic, and had significantly longer axial lengths than those who showed the other patterns ($P < 0.0001$, one-factor ANOVA).

A total of 66 of 367 eyes were excluded from the measurements of the central retinal thickness: 45 eyes due to myopic traction maculopathy (MTM), 18 eyes due to myopic CNV, 1 eye due to macular atrophy, and 2 eyes due to macular holes. In the end, the central retinal thickness was measured in 301 of 367 eyes. The central retina was significantly thinner in eyes with irregular curvature than in eyes with any other pattern ($P < 0.0001$, one-factor ANOVA).

The subfoveal scleral thickness was measurable in 13 of 44 eyes (29.5%) with a curve that sloped toward the optic disc, in 55 of 98 eyes (56.1%) with symmetrical curvature, in 58 of 105 eyes (55.2%) with asymmetrical curvature, and in 113 of 120 eyes (94.2%) with irregular curvature. The subfoveal sclera was thinnest in the eyes with irregular curvature, followed by the eyes with symmetrical curvature, those with asymmetrical curvature, and those with curvature toward the optic disc. A statistical comparison of the subfoveal scleral thickness among the groups was not performed because it was not possible to measure the subfoveal scleral thickness in 130 of the eyes.

The subfoveal choroid was too thin to be measured in 45 of 98 eyes (45.9%) with symmetrical curvature, in 55 of 105 eyes (52.4%) with asymmetrical curvature, in 11 of 44 eyes (25.0%) with curvature sloping toward the optic disc, and in all 120 eyes with irregular curvature. Statistical analyses showed that the number of eyes whose choroid was too thin to be measured was significantly greater among eyes with irregular curvature than in any other group ($P < 0.0001$, χ^2 tests). Also, the number of eyes whose choroid was too thin to be measured was significantly lower among eyes with curvature sloping toward the optic disc than in any other group ($P < 0.0001$, χ^2 tests).

Correlation between Curvature of Inner Scleral Surface and Myopic Fundus Lesions

In 367 of 488 highly myopic eyes in which the contour of the inner sclera was analyzed, the prevalence of a posterior staphyloma, MTM, myopic chorioretinal atrophy, and myopic CNV was 90.7% (333 eyes), 49.9% (183 eyes), 31.6% (116 eyes), and 15.3% (56 eyes), respectively. A posterior staphyloma was found in all 105 eyes with an asymmetrical curvature and in all 120 eyes with an irregular curvature (Table 3). These numbers were significantly higher than in eyes with symmetric curvature or with curvature sloping toward the optic disc ($P < 0.001$, Fisher's exact probability tests). On the other hand, a staphyloma was present in 26 of 44 eyes (59.0%) whose curvature slopped toward the optic disc, which was significantly fewer than in other groups ($P < 0.05$, Fisher's exact probability tests).

Table 3. Comparison of Characteristics between Highly Myopic Eyes with Different Contours of Inner Scleral Surface in Radial Scans Centered on the Fovea

	Incline toward the Optic Disc	Symmetrical, Centered on the Fovea	Asymmetrical, Fovea on the Slope	Irregular Curve	*P* Value
No. of eyes (No. of persons)	44 (30)	98 (72)	105 (75)	120 (85)	
Age, y, mean ± SD	51.3 ± 14.8 (20–74)	53.7 ± 14.1 (12–82)	56.9 ± 14.2 (12–81)	63.3 ± 10.7 (32–89)	<0.0001*
Refractive error, d, mean ± SD	−11.9 ± 3.2 (−8.5 to −20.0)	−12.9 ± 3.5 (−8.5 to −24.0)	−12.6 ± 4.5 (−8.5 to −25.5)	−16.2 ± 3.9 (−10.0 to −23.0)	<0.0001*
Axial length, mm, mean ± SD	29.2 ± 1.6 (26.6–33.4)	29.6 ± 1.9 (26.5–34.3)	29.2 ± 1.9 (26.5–36.2)	31.0 ± 1.6 (27.7–36.6)	<0.0001*
Central retinal thickness, μm, mean ± SD	178.3 ± 42.3 (95–242)	183.6 ± 28.7 (82–211)	152.0 ± 38.9 (52–253)	130.1 ± 33.2 (59–205)	<0.0001*
Subfoveal scleral thickness, μm, mean ± SD (No. of eyes whose scleral thickness was measurable)	279.7 ± 111.2 (146–477) (13)	240.9 ± 76.5 (118–528) (55)	276.4 ± 78.5 (146–546) (58)	189.1 ± 60.9 (80–380) (113)	<0.0001*
Posterior staphyloma, No. of eyes (%)					
Present	26 (59.0%)	82 (83.7%)	105 (100%)	120 (100%)	
Absent	18 (40.9%)	16 (16.3%)	0 (0%)	0 (0%)	
MTM, No. of eyes (%)	5 (11.4%)	34 (34.7%)	53 (50.5%)	91 (75.8%)	<0.0001†
Myopic chorioretinal atrophy, No. of eyes (%)	15 (11.4%)	15 (15.3%)	16 (15.2%)	70 (58.3%)	<0.0001†
Myopic CNV, No. of eyes (%)	4 (9.1%)	8 (8.2%)	11 (10.5%)	33 (27.5%)	0.004†

* One-factor ANOVA.
† χ^2 tests.

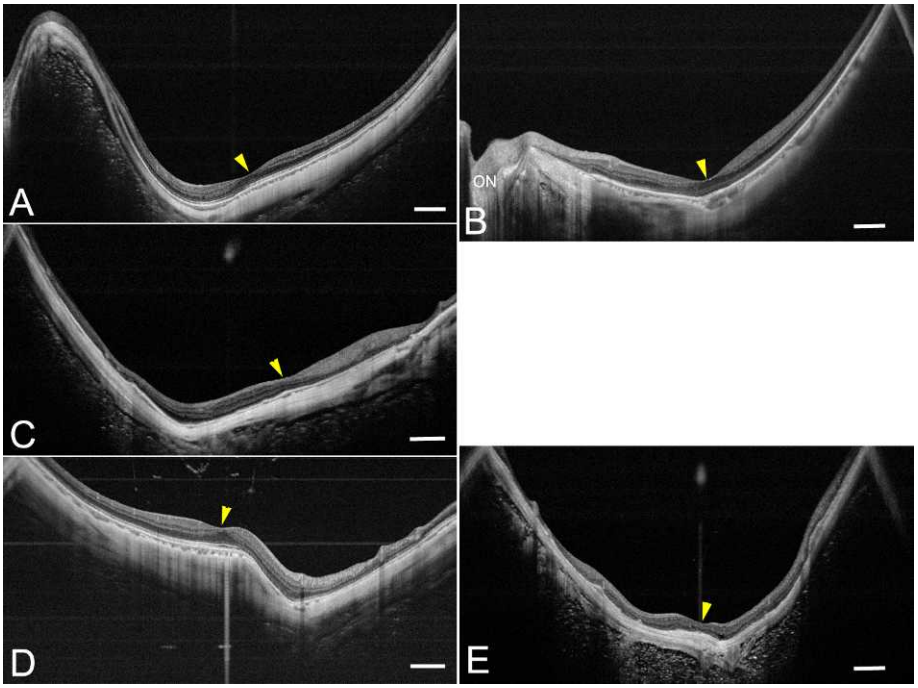

FIGURE 5. Different patterns of scleral curvature in eyes classified with irregular curvature. (**A**) The sclera nasal to the most protruded point is extremely thin and the scleral curvature is not spherical. The central fovea is on the slope (*arrowhead*). (**B**) The scleral curvature is bent at the site of the central fovea (*arrowhead*). (**C**) The scleral curvature is similar to that in (**A**); however, the curvature is more linear and the transition of the change in curvature is more acute. The central fovea is on the slope (*arrowhead*). (**D**) The scleral thickness is irregular and the sclera is acutely displaced posteriorly beside the central fovea shown by the *arrowhead*. (**E**) The sclera is extremely thin and the scleral curvature is entirely irregular. The central fovea (*arrowhead*) is almost centered in the irregular curvature.

Chorioretinal atrophy, patchy atrophy or macular atrophy, and myopic CNVs were observed significantly more frequently in eyes with irregular curvature than in any other group ($P < 0.0001$ and $P = 0.004$, respectively, χ^2 tests, Table 3). MTM was observed most frequently in eyes with irregular curvature, followed by those with asymmetrical curvature, those with symmetrical curvature, and those with a curvature that sloped toward the optic disc.

Determination of Location of Most Protruded Part of Highly Myopic Eyes with Asymmetric or Irregular Curvature

In eyes with symmetrical curvature, the central fovea sat at the bottom of the curvature of posterior segments of the eye. In eyes where the curvature sloped toward the optic disc, the optic disc was also at the bottom of the curvature.

We were able to determine the location of the most protruded part in the posterior segment in 105 eyes with asymmetric curvature and 120 eyes with irregular curvature (see Supplementary Material and Supplementary Table S1, http://www.iovs.org/lookup/suppl/doi:10.1167/iovs.12-10161/-/DcSupplemental). The most protruded point existed somewhere other than in the central fovea or optic disc in the eyes with an asymmetric curvature; the location of the most protruded part was not consistent in the eyes with irregular curvature. For our analyses, we combined the superior, temporal superior, and nasal superior into one group called the "upper" and combined the inferior, temporal inferior, and nasal inferior into one group called the "lower" (Fig. 1B). Our analyses showed that the lower area was the most protruded part both in eyes with asymmetric curve and in eyes with irregular curve (85.7% and 58.3%, respectively). In 85.7% of the eyes with asymmetric curvature, the most protruded part existed inferior to the fovea (see Supplementary Material and Supplementary Table S1, http://www.iovs.org/lookup/suppl/doi:10.1167/iovs.12-10161/-/DcSupplemental). On the other hand, the most protruded part existed in the central fovea in 28.4% of the eyes with irregular curvature. The curvature was too irregular to allow identification of the most protruded part in five eyes, and three of these eyes had macular intrachoroidal cavitation (ICC)[25] and were excluded from the analyses.

A summary of the relationship between the location of the most protruded point and the curvature of the sclera is presented in Supplementary Table S2 (see Supplementary Material and Supplementary Table S2, http://www.iovs.org/lookup/suppl/doi:10.1167/iovs.12-10161/-/DcSupplemental).

Distance and Depth of Most Protruded Part in Posterior Fundus Away from Central Fovea

The most protruded point existed away from the central fovea in all 103 eyes with asymmetrical curvature (after 2 eyes with macular ICC were excluded from the 105 eyes) and in 81 of 114 eyes with irregular curvature (after 1 eye with macular ICC and 2 eyes whose curve was too irregular for identification of the most protruded point were excluded) (see Supplementary Material and Supplementary Tables S1 and S2, http://www.iovs.org/lookup/suppl/doi:10.1167/iovs.12-10161/-/DcSupplemental). In these 184 eyes, the average distance between the most protruded part and the central fovea was 2020.1 ± 632.1 μm (772–4153 μm). The average depth of the most protruded point from the foveal plane was 251.2 ± 164.3 μm (51–978 μm). The average distance of the most protruded point from the central fovea was 2092.6 ± 675.9 μm (846–4153 μm) in the eyes with asymmetrical curvature and 1847.8 ± 565.7 μm (901–3480 μm) in eyes with irregular curvature. The most protruded point in the eyes with asymmetric curve was situated farther away from the fovea than in the eyes with

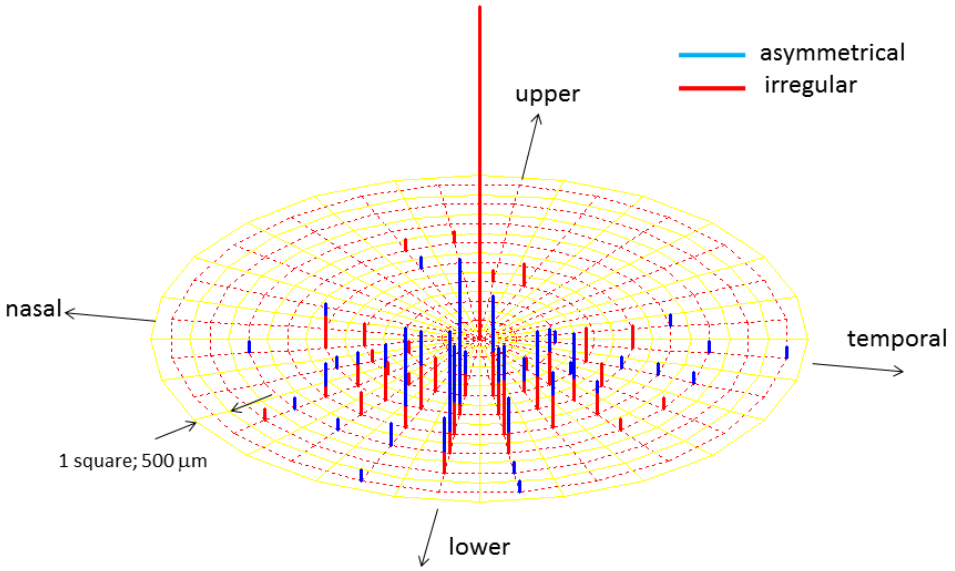

Figure 6. Topographic map of the distribution of the most protruded point relative to the location of central fovea in eyes with asymmetric or irregular scleral curvature. The most protruded part was identified in each of 12 radial scans centered on the central fovea, and the depth of the most protruded part from the foveal plane was measured in each scan. Then, the scan that included the most protruded part whose depth from the foveal plane was the greatest was determined. The distance of the most protruded point from the fovea was measured with the caliper function of the built-in software of swept-source OCT. The center of this graph is the central fovea. The distribution of the most protruded point is expressed on each meridian centered on the fovea according to its orientation and distance from the fovea. The *red bar* means that the eye belongs to the asymmetrical curvature group; the *blue bar* means that the eye belongs to the irregular curvature group. Each square shows 500 μm in distance.

irregular curve ($P = 0.004$, Mann-Whitney U tests). The average depth of the most protruded point from the foveal plane was 236.8 ± 155.8 μm (51–978 μm) in the eyes with asymmetrical curvature and 235.7 ± 139.5 μm (73–772 μm) in the eyes with irregular curvature. The frequency and distribution of the most protruded point in the eyes with asymmetrical curvature or with irregular curvature as a function of the distance and depth of the most protruded point from the fovea are plotted in Figure 6.

Twenty-eight highly myopic eyes with TDS were examined by swept-source OCT. To determine the difference in the curvature of the posterior segment of highly myopic eyes with and without TDS, we compared the location and depth of the most protruded part between these two groups. The clinical characteristics of the patients with TDS are shown in Supplementary Table S3 (see Supplementary Material and Supplementary Table S3 http://www.iovs.org/lookup/suppl/doi:10.1167/iovs.12-10161/-/DcSupplemental).

Among the 28 eyes with TDS, the most protruded part existed inferior to the central fovea in 21 eyes (75.0%), temporally inferior to the fovea in 4 eyes (14.3%), and nasally inferior in 3 eyes (10.7%). In the 28 eyes with TDS, the average distance of the most protruded point from the central fovea was 2992.5 ± 830.7 μm (1956–4591 μm), and the average depth of the most protruded point from the foveal plane was 673.5 ± 263.7 μm (314–1292 μm). Statistical analyses showed that the most protruded point was significantly more distant from the central fovea in the highly myopic eyes with TDS than in those without TDS ($P < 0.0001$, Mann-Whitney U tests). In addition, the depth of the most protruded point from the foveal plane was significantly greater in the eyes with TDS than in those without ($P < 0.0001$, Mann-Whitney U tests).

Scleral Thickness of Most Protruded Part Away from Central Fovea

The average scleral thickness at the most protruded part of the posterior segment was 155.8 ± 55.8 μm (52–303 μm) in all 184 eyes whose most protruded point was outside the central fovea. In eyes with asymmetric curvature, the average scleral thickness at the most protruded part was 185.2 ± 55.9 μm (96–303 μm); and in eyes with irregular curvature, it was 130.8 ± 40.0 μm (52–243 μm). Statistical analyses showed that the scleral thickness at the most protruded point was significantly less in eyes with irregular curvature than in those with asymmetric curvature ($P < 0.0001$, Welch's t-tests).

We then compared the scleral thickness at the most protruded part and the thickness at other areas. In the eyes with asymmetric curvature, the scleral thickness at the most protruded part was significantly less than the subfoveal scleral thickness and that nasal to the fovea ($P < 0.05$, Dunn's multiple comparison test). However, the differences between the thickness at the most protruded part and that temporal to the fovea or that inferior to the fovea were not significant. In the eyes with irregular curvature, the scleral thickness at the most protruded part was significantly less than the thickness of the subfoveal sclera, that nasal to the fovea, and that superior to the fovea ($P < 0.05$, Dunn's multiple comparison test). However, the differences in the thickness between the most protruded part and that temporal to the fovea or between the most protruded part and that inferior to the fovea were not significant.

Correlation between Shape of Globe Determined by 3D MRI and Contour of Inner Scleral Surface Determined by OCT

Forty-three patients (70 eyes) agreed to undergo a 3D MRI examination according to the protocol we reported previously.[11] Written informed consent was obtained from each patient for the 3D MRI examination. The results are summarized in Table 4. The degree of symmetry of the posterior eye segment in the horizontal and sagittal planes, as well as the pointedness of the posterior pole of the eye, was analyzed in the 3D MRIs (Fig. 2). Although statistical analyses were not performed due to the limited number of

Table 4. Correlation between Eye Shape Examined by 3D MRI and Curvature of the Posterior Segment of the Eye by OCT

3D MRI Analyses*	Incline toward the Optic Disc (5 eyes)	Symmetrical, Centered on the Fovea (16 eyes)	Asymmetrical, Fovea on the Slope (24 eyes)	Irregular Curve (25 eyes)
Symmetricity in horizontal plane				
Symmetrical	0 eyes (0%)	16 eyes (100%)	21 eyes (87.5%)	16 eyes (64.0%)
Nasally distorted	5 eyes (100%)	0 eyes (0%)	3 eyes (12.5%)	7 eyes (28.0%)
Temporally distorted	0 eyes (0%)	0 eyes (0%)	0 eyes (0%)	2 eyes (8.0%)
Symmetricity in sagittal plane				
Symmetrical	2 eyes (40.0%)	12 eyes (75.0%)	11 eyes (45.8%)	13 eyes (52.0%)
Inferiorly distorted	3 eyes (60.0%)	3 eyes (18.8%)	14 eyes (58.3%)	12 eyes (48.0%)
Superiorly distorted	0 eyes (0%)	1 eye (6.3%)	0 eyes (0%)	0 eyes (0%)
Sharpness of posterior segment of the eye				
Pointed	2 eyes (40.0%)	2 eyes (12.5%)	10 eyes (41.7%)	18 eyes (72.0%)
Dull	3 eyes (60.0%)	14 eyes (87.5%)	14 eyes (58.3%)	7 eyes (28.0%)

* See Methods for details.

eyes analyzed by 3D MRI, there was some tendency for the shape as determined by 3D MRI to fall into the four distinct patterns of curve of the inner scleral surface. Among the eyes with scleral curvature inclined toward the optic disc, all were not horizontally symmetrical and all were the nasally distorted type. Among the eyes with symmetrical curvature, all were horizontally symmetrical and 75% were sagittally symmetrical as well. Among eyes with asymmetric curvature, horizontal symmetry was found in 87.5%; however, the number of eyes with sagittal symmetry decreased to 45.8%, and 58.3% of the eyes had the inferiorly distorted shape. Among eyes with irregular curvature, horizontal symmetry was observed in 64.0%, and the temporally distorted type was identified only in this group.

Regarding the sharpness of the posterior segment of the eyes, the pointed shape was observed significantly more

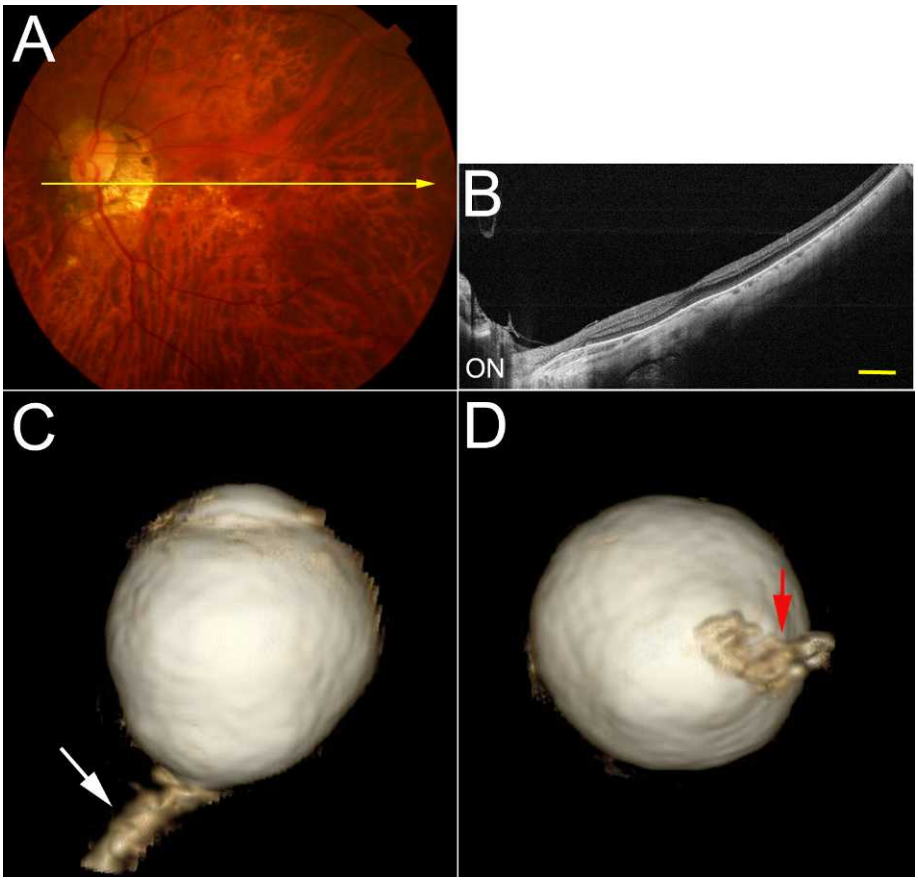

Figure 7. Relationship between highly myopic eyes with the scleral curvature sloped toward the optic nerve by OCT and nasally distorted eye by 3D MRI. (**A**) Left fundus of a 71-year-old woman with myopic refractive error of −9.5 diopters and an axial length of 26.6 mm. The fundus photograph shows a ring conus around the optic disc and mild chorioretinal atrophy in the macula. *Yellow line* shows a scanned line by OCT in (**B**). (**B**) Image from a horizontal OCT scan shows that the retinal pigment epithelium (RPE) and the curvature of the inner scleral surface are almost straight and are sloped toward the optic nerve (ON). *Scale bar* = 1 mm. (**C**) Inferior view of a 3D MRI image of the eye shows that the globe is elongated slightly nasally and that the optic nerve (*arrow*) is attached at the most protruded part of the globe. (**D**) Posterior view of 3D MRI image of the eye shows that the optic nerve (*arrow*) is attached at the center of the protrusion of the globe.

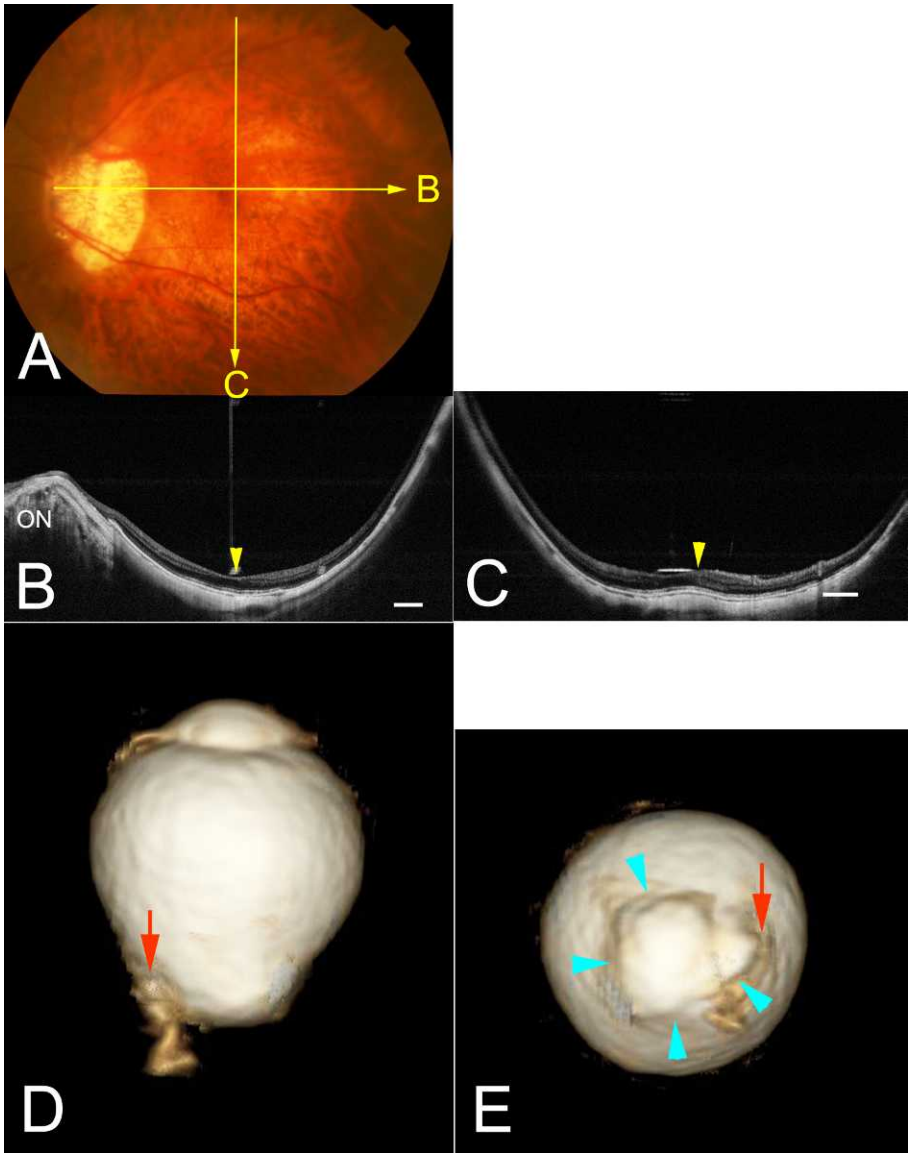

Figure 8. OCT image of highly myopic eye with a symmetrical curvature of the sclera centered on the fovea, and 3D MRI image of the same eye showing symmetrical elongation both horizontally and sagittally. (**A**) Photograph of the fundus of the left eye of a 70-year-old man with myopic refractive error of −15.0 diopters and an axial length of 29.5 mm. Photograph shows a temporal conus with a marked tilting of the optic disc. Mild chorioretinal atrophy is seen in the macula. *Yellow lines* show scanned lines by OCT in (**B**) and (**C**). (**B**, **C**) Horizontal (**B**) and vertical (**C**) scans showing that the curvature of the inner scleral surface is symmetrical around the central fovea (*arrowhead*). ON, optic nerve. *Scale bar* = 1 mm. (**D**) Inferior view of 3D MRI image of the eye shows that the globe is elongated symmetrically in the horizontal plane. The optic nerve (*arrow*) is attached nasal to the protrusion of the globe. (**E**) Posterior view of 3D MRI image of the eye shows that the protrusion (*arrowheads*) is almost centered horizontally and vertically. The optic nerve (*arrow*) is attached nasal to the protrusion.

frequently (75.0%) in eyes with irregular curvature whereas the dull shape was always dominant in the other three groups.

Representative cases with the four different types of curvatures of the inner scleral surface are shown in Figures 7 through 10.

Discussion

Examinations of highly myopic eyes by swept-source OCT showed that the entire layer of the sclera appeared as a uniform hyperreflective structure. The outer boundary of the sclera was clearly seen in 57% of 488 highly myopic eyes. In some cases, even Tenon's capsule and the episclera, which is composed of irregularly arranged collagen fibers,[30] were observed outside the sclera. The swept-source OCT images clearly showed that the connective tissue fibers of Tenon's capsule spread and blended into the orbital fat posteriorly.

Statistical analyses showed that many factors, for example age, axial length, staphyloma, central retinal thickness, and thinness of the choroid, were significantly correlated with the visibility of the entire scleral layer. Multiple regression analyses were not performed because the objective variable, the visibility of entire layer of sclera, was not a continuous variable. Thus, we could not determine which factors affected the visibility of the outer border of the sclera most significantly. In addition, it is possible that some of these factors might be correlated with each other as reported in part by Fujiwara et al.,[31] who found a significant correlation between macular choroidal thickness and age and refractive error. It is likely that an increase in age and axial length causes a decrease

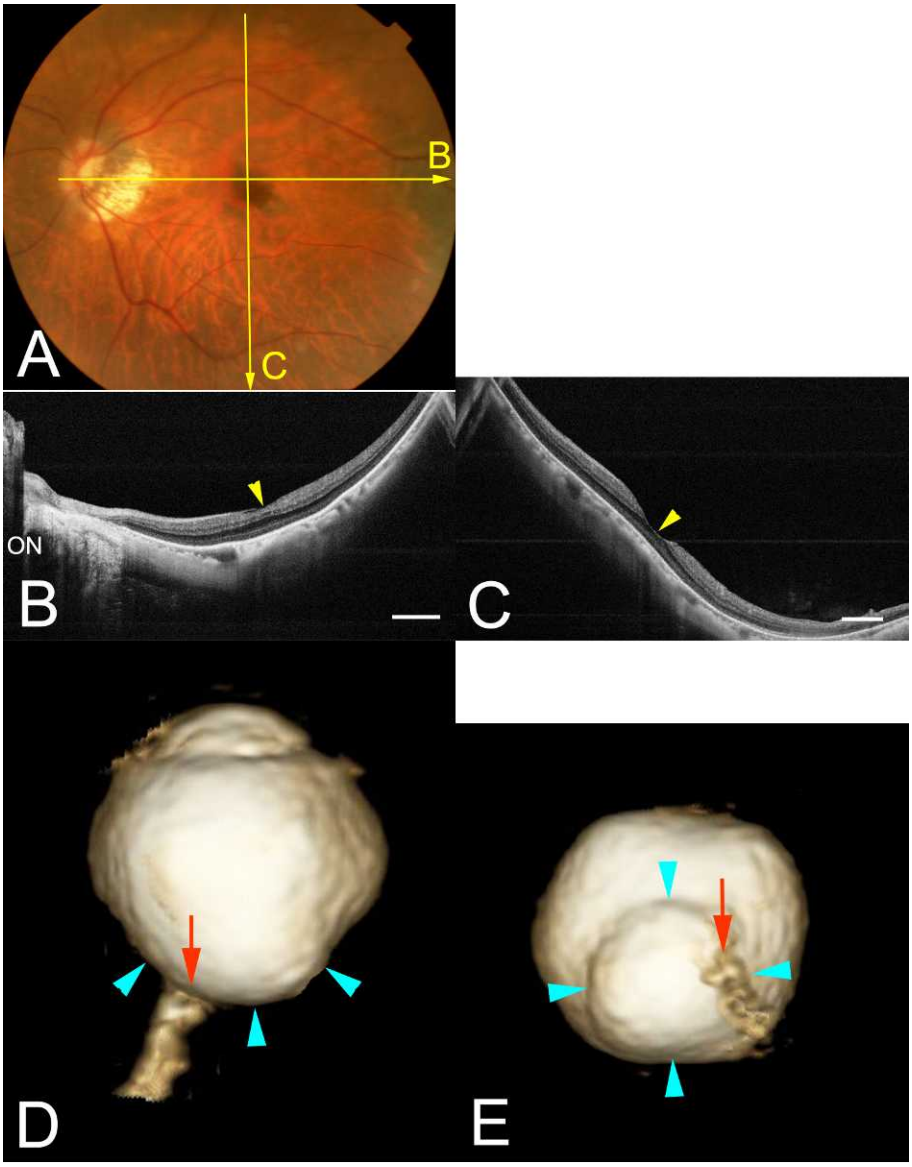

Figure 9. OCT image of a highly myopic eye with asymmetrical curvature of the sclera and 3D MRI image of the same eye showing an inferiorly distorted eye. (**A**) Photograph of the left fundus of a 68-year-old woman with an axial length of 28.2 mm (intraocular lens–implanted eye) showing a temporal conus around the optic disc. *Yellow lines* show scanned lines by OCT in (**B**) and (**C**). (**B**) Horizontal OCT scan showing that the most protruded point is slightly nasal to the central fovea (*arrowhead*). ON, optic nerve. *Scale bar* = 1 mm. (**C**) Vertical OCT scan showing that the most protruded point is inferior to the central fovea. The fovea (*arrowhead*) is on the slope. *Scale bar* = 1 mm. (**D**) Inferior view of 3D MRI image of the eye shows that the globe is elongated symmetrically in the horizontal plane. The optic nerve (*arrow*) is situated within the protrusion shown by the arrowheads. (**E**) Posterior view of 3D MRI image of the eye shows that the protrusion (*arrowheads*) is located inferiorly. The optic nerve (*arrow*) is located within the nasal margin of the protrusion.

in thickness of the retina and choroid in the area of a posterior staphyloma, and this could affect the visibility of entire scleral layer.

Our results showed that the average subfoveal scleral thickness in 278 highly myopic eyes without a DSM was 228 μm. Curtin[14] used histological studies to show that the scleral thickness at the posterior pole of normal eyes with axial lengths between 22 and 24 mm was 660 μm, whereas it was 233 μm in myopic eyes with an axial length of 27.8 mm. A PubMed search identified only one article whose authors had measured the scleral thickness in highly myopic eyes.[21] Imamura et al.[21] used EDI-OCT to show that the mean subfoveal scleral thickness in 25 highly myopic eyes without a DSM and a mean refractive error of −11.7 ± 5.5 D was 281 ± 85 μm. The values measured histologically[9] and by EDI-OCT[21] are comparable to the values we found.

The measurement of scleral thickness in different areas showed that the sclera was thickest 3000 μm nasal to the central fovea, followed by the subfoveal area and then by the areas temporal, superior, and inferior to the fovea. In 29 eyes with type IX staphyloma, the sclera 3000 μm nasal to the fovea was too thick to measure because of the scleral ridge that is characteristic of type IX staphyloma.[12,29] Imamura et al.[21] reported that the average scleral thickness 3000 μm temporal to the fovea was 320 μm in highly myopic eyes without DSM; this was greater than the subfoveal scleral thickness (281 μm) in the same patients. The reason for the discrepancy between their results and ours was not determined; however, one possibility might be that we studied more severely myopic eyes with irregular curvature of sclera. Our results suggested the possibility that in highly myopic eyes without evidence of

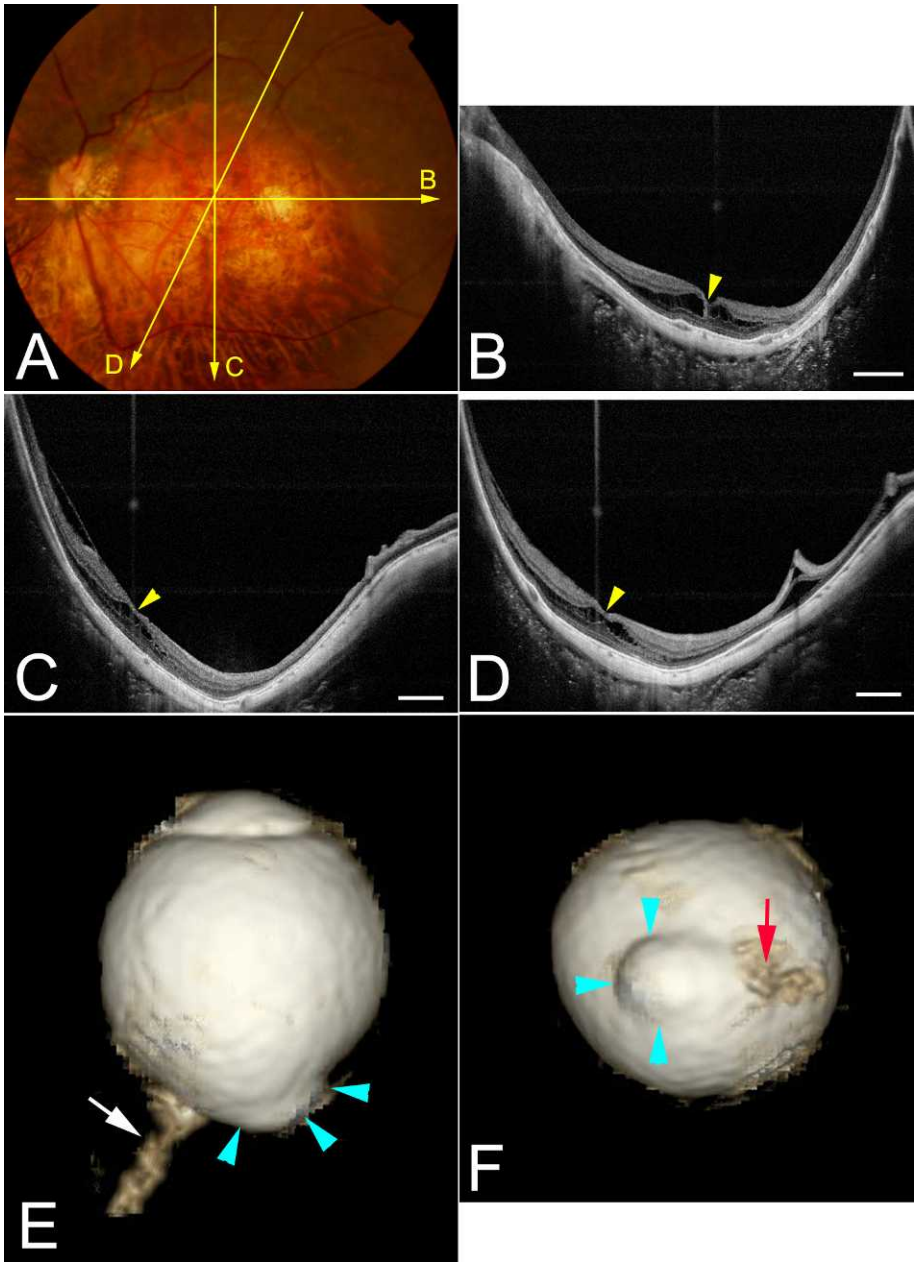

Figure 10. OCT image of a highly myopic eye with irregular curvature of the sclera and 3D MRI image showing temporally distorted eye. (**A**) Photograph of the left fundus of a 74-year-old woman with an axial length of 32.4 mm (intraocular lens–implanted eye) showing severe chorioretinal atrophy in the macula. *Yellow lines* show scanned lines by OCT in (**B**), (**C**), and (**D**). (**B**) Horizontal OCT image showing that the sclera is thin and is not spherical. The orbital fat tissue is clearly seen posterior to the sclera. Macular retinoschisis is seen around the central fovea (*arrowhead*). *Scale bar* = 1 mm. (**C**, **D**) OCT image from a vertical scan (**C**) and image from an oblique scan (**D**). The scleral contour is not spherical, and the most protruded point is located inferior to the central fovea (*arrowhead*). Macular retinoschisis can also be seen. *Scale bars* = 1 mm. (**E**) Inferior view of 3D MRI image of the eye shows that the posterior segment of the globe is temporally dislocated. The optic nerve (*arrow*) is attached nasal to the protrusion (*arrowheads*) of the globe. (**F**) Posterior view of 3D MRI image of the eye shows that the optic nerve (*arrow*) is attached nasal to the protrusion (surrounded by *arrowheads*).

DSM, the subfoveal sclera is thicker than the sclera temporal, inferior, and superior to the fovea. This needs to be confirmed in a larger population including persons with less myopic eyes.

While the curvature of the RPE and Bruch's membrane had two distinct patterns in emmetropic eyes (Figs. 4A–D), the curvature of the inner scleral surface was consistently symmetrical around the central fovea. On the other hand, the curvature of the inner scleral surface was almost identical to that of the RPE and Bruch's membrane in highly myopic eyes, mainly due to a very thin choroid situated between Bruch's membrane and the sclera.

In highly myopic eyes, the curvature of the inner scleral surface in the posterior segment of the eye had four distinct patterns: symmetrical around the central fovea, sloping toward the optic disc, asymmetrical around the fovea, and irregular curvature. The first two patterns appeared to be similar to the contour of the RPE and Bruch's membrane in emmetropic eyes, although the degree of curvature was greater in the highly myopic eyes. These findings suggested the possibility that the symmetrical shape around the fovea and sloping toward the optic disc might be an exaggerated form of the

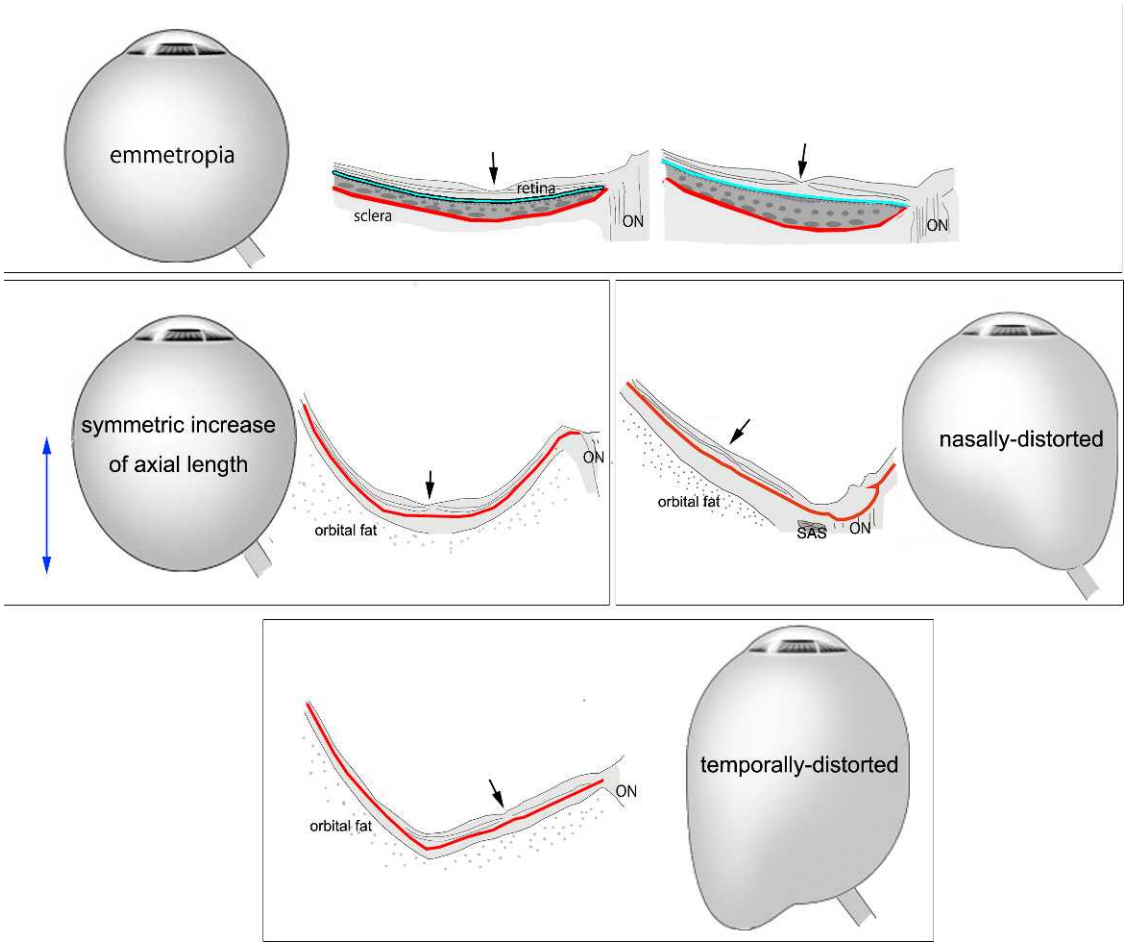

Figure 11. Schematic illustration of our hypothesis on how eye deformities in the horizontal plane progress in pathologic myopia, based on 3D MRI image and the results obtained by swept-source OCT. *Top row*: Emmetropic eyes. There are two different curvature patterns of the RPE and Bruch's membrane (shown as *blue line*) in emmetropic eyes: straight sloping of the sclera toward the optic nerve and mildly bowed centered on the fovea. However, the curvature of the inner scleral surface (*red line*) is mildly bowed posteriorly and always symmetrical around the fovea. This is due to the thick choroid affecting the curvature of the inner scleral surface in emmetropic eyes. *Middle row, left*: Symmetrically elongated highly myopic eye. When the eye elongates around the fovea, the symmetric curve of sclera seen in emmetropic eyes is exaggerated. The central fovea is on the most protruded point of the sclera. *Middle row, right*: Nasally dislocated eye in high myopia. When the eye elongated toward the optic nerve, the curvature of the inner scleral surface had an exaggeration of the RPE and Bruch's membrane slope as seen in the *top row, right* figure. The curvature of the inner scleral surface is almost straight and sloped toward the optic nerve. *Bottom row*: Temporally dislocated eye in high myopia. When the sclera thins and expands further in extremely myopic eyes, the very thin sclera can no longer maintain the curvature, and an irregular curvature results as seen in the OCT image. The area temporal to the central fovea appears to expand more and shows a temporally dislocated type by 3D MRI of the globe. The curvature of the inner scleral surface is shown as a *red line*, and the central fovea is shown by an *arrowhead* in each image. ON, optic nerve; SAS, subarachnoid space.

normal curvature of the RPE and Bruch's membrane seen in emmetropic eyes. In highly myopic eyes with very thin choroid, the scleral curvature was almost identical to the RPE curve. We suggest that when an eye elongates without forming a staphyloma, the patterns may be the same as seen in emmetropic eyes but more exaggerated in highly myopic eyes.

On the other hand, the asymmetrical and irregular patterns were observed only in highly myopic eyes. In the eyes with asymmetrical curvature around the central fovea, the most protruded point was almost always present inferiorly, including temporally inferior and nasally inferior to the fovea (see Supplementary Material and Supplementary Table S1, http://www.iovs.org/lookup/suppl/doi:10.1167/iovs.12-10161/-/DcSupplemental; Fig. 6). The fovea in these eyes was located on the superior slope of the curvature. All of the eyes with asymmetrical curvature had a staphyloma that was seen significantly more frequently than in eyes with symmetrical curvature or curvature sloping toward the optic disc. We have reported that the most protruded part of the eye existed along the visual axis in 78% of the highly myopic eyes, and inferior to the central axis in 22% of the eyes in the 3D MRI images.[11] These findings indicate that the inferior sclera expands more in highly myopic eyes. The sclera in the lower half of the eye is the area where the embryonic ocular fissure closes, and thus it might be possible that this part of the sclera is structurally weaker than the other areas. This also suggests some similarities between pathologic myopia and TDS, although the posterior bulge existed more peripherally in the inferior fundus and the degree of bulge was greater in eyes with TDS than in highly myopic eyes without evidence of the TDS. During the development of a staphyloma, the greater expansion of the inferior sclera compared to other parts of the sclera might cause a shift of the most protruded part from the subfovea to the inferior fundus, and in turn the fovea might be shifted onto the upper slope of the sclera (Fig. 11).

In the eyes with irregular curvature of the sclera, the most protruded point existed in the fovea in 28% and in the inferior fundus in 58% of the eyes (see Supplementary Material and

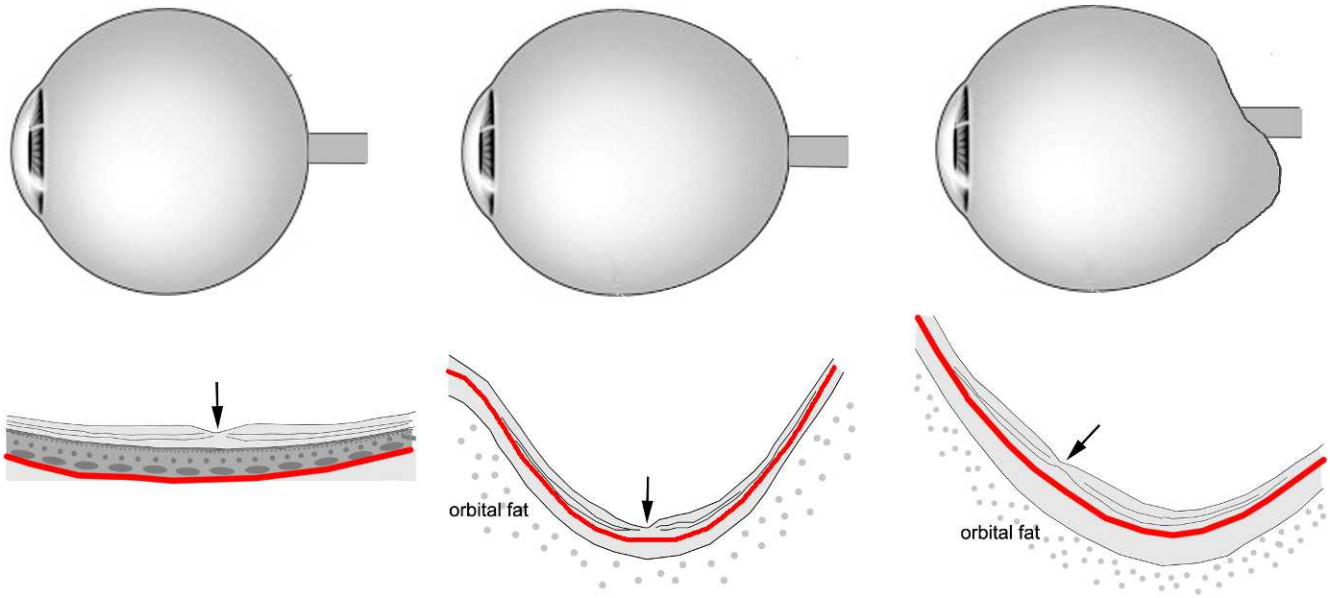

Figure 12. Schematic illustrations of our hypothesis on how eye deformities in the sagittal plane progress in pathologic myopia based on 3D MRI images and the images of swept-source OCT vertical scans. *Left*: Emmetropic eye. The globe is spherical by 3D MRI, and the vertical OCT scan shows that the curvature of the inner scleral surface is mildly bowed and symmetrical around the central fovea. *Middle*: Symmetrically elongated highly myopic eye. When the eye simply elongates along the central axis, the symmetrical curvature of the sclera seen in emmetropic eyes is exaggerated. The scleral curvature is bowed more posteriorly, and the central fovea is on the most protruded point of the sclera. *Right*: Inferiorly distorted eye with high myopia. When a posterior staphyloma develops in later life, the posterior sclera is expanded nonuniformly, and the lower sclera tends to be expanded more than other parts of the sclera. This causes a shift of the most protruded point from the subfovea to the lower fundus, and the fovea tends to move onto the upper slope. The curvature of the inner scleral surface is shown as a *red line*, and the central fovea is shown by an *arrowhead* in each image.

Supplementary Table S1, http://www.iovs.org/lookup/suppl/doi:10.1167/iovs.12-10161/-/DcSupplemental; Fig. 6). The patients whose eyes had an irregular curvature were significantly older; and their eyes were more myopic, had longer axial lengths, and had thinner central retinal thickness than any of the other types (Table 3). Also, the subfoveal sclera was significantly thinner, as thin as 189 μm, in the eyes with irregular curvature compared to other groups.

The myopic fundus lesions, for example, chorioretinal atrophy, CNV, and MTM, were observed significantly more frequently in eyes with irregular curvature than in those with any other type of scleral curvature. We suggest that when the sclera is stretched and becomes extremely thin, it can no longer maintain its normal curvature, and this would contribute to the development of myopic fundus lesions. Thus, irregular curvature might be the most severe and advanced form of pathologic myopia.

Finally, we compared the shape of the eye determined by 3D MRI and the contour of the inner scleral surface determined by OCT (Table 4, Figs. 7–10). The results showed that all the eyes with a curvature sloping toward the optic disc by OCT were nasally distorted as evidenced by MRI according to our definition[11] (Table 4, Fig. 7). Seventy-five percent of the eyes with symmetrical curvature by OCT were also symmetrical horizontally and sagittally in the MRI images (Table 4, Fig. 8). Horizontal symmetry was less frequent in eyes with irregular curvature (Table 4), and the temporally distorted type was observed only in eyes with irregular curvature. We have reported that significant visual field defects[7] not explained by myopic fundus lesions were observed significantly more frequently in temporally distorted eyes than in other types (nasally distorted, cylinder, or barrel type).[11] Also, among eyes with irregular curvature, those with a pointed posterior pole were observed more frequently than those with the dull shape. We recently found that the posterior pole of highly myopic eyes becomes more pointed as patients age (unpublished data). Probably the development and increase in depth of the staphylomas are the cause for the increased pointedness.

When the results of 3D MRI analyses and OCT findings are combined, the temporally dislocated types might represent a condition in which the sclera is extremely thinned and becomes irregular in contour at an advanced stage of pathologic myopia with a deep staphyloma. In fact, 46% of the eyes with asymmetrical curvature were judged to be symmetrical in both the horizontal and sagittal planes by 3D MRI. These findings suggest a possibility that swept-source OCT might be able to detect more minute and subtle deformities of the posterior segments of the eye than MRI, although the scanned area is limited. It would be the best to use both swept-source OCT and 3D MRI to analyze the shape of the globe.

Schematic illustrations of our hypothesis on how the eye deformities progress in pathologic myopia, based on the 3D MRI findings in our earlier study[11] and the swept-source OCT results in this study, are shown in Figures 11 and 12. Despite the two different curvatures of the RPE and Bruch's membrane in emmetropic eyes, the curvature of the inner scleral surface was mildly bowed posteriorly and consistently symmetrical around the fovea (Fig. 12, top row). When the eye simply elongates around the fovea or elongates toward the optic nerve, the curvature of the inner scleral surface as well as the curvature of Bruch's membrane in highly myopic eyes had an exaggeration of the patterns of the RPE and Bruch's membrane curvature seen in emmetropic eyes (Fig. 12, middle row).

When a posterior staphyloma develops in later life, the posterior sclera is expanded in a nonuniform fashion, and the lower sclera tends to expand more than other parts of the sclera (Fig. 11, right). This causes a shift of the most protruded point from the subfovea to the inferior fundus, and the fovea tends to move onto the superior slope. When the sclera thins and expands further in extremely myopic eyes, the very thin sclera can no longer maintain the curvature, and this results in

an irregular curvature (Fig. 12, bottom row). A long-term study on the course of deformation of eyes with pathologic myopia is necessary to support our hypothesis.

There are several limitations to this study. The study was conducted in the High Myopia Clinic at our university. Thus, the results might not reflect the tendency in the general myopic population. Also, 3D MRI analyses were performed in a limited number of patients who agreed to the MRI examination. Thus, the data obtained through comparison of the 3D MRI and OCT images might not apply to the rest of our highly myopic patients. Also, eyes with DSM were excluded from the analyses of scleral curvature.

Despite all of these limitations, we believe that our results obtained by swept-source OCT provide important information on the in situ shape of the sclera and the differences in the scleral curvature in highly myopic eyes. We conclude that swept-source OCT is a powerful tool to examine deeper tissues of the eye in situ, and use of this tool can provide information on how specific patterns of scleral curvatures could damage the macula and optic nerve, which can then lead to the vision-threatening complications in pathologic myopia.

Acknowledgments

The authors thank Duco Hamasaki for his critical discussion and final manuscript revision.

References

1. Green JS, Bear JC, Johnson GJ. The burden of genetically determined eye disease. *Br J Ophthalmol*. 1986;70:696–699.
2. Krumpaszky HG, Ludtke R, Mickler A, Klauss V, Selbmann HK. Blindness incidence in Germany. A population-based study from Wurttemberg-Hohenzollern. *Ophthalmologica*. 1999; 213:176–182.
3. Munier A, Gunning T, Kenny D, O'Keefe M. Causes of blindness in the adult population of the Republic of Ireland. *Br J Ophthalmol*. 1998;82:630–633.
4. Cotter SA, Varma R, Ying-Lai M, Azen SP, Klein R. Causes of low vision and blindness in adult Latinos: the Los Angeles Latino Eye Study. *Ophthalmology*. 2006;113:1574–1582.
5. Buch H, Vinding T, La Cour M, Appleyard M, Jensen GB, Nielsen NV. Prevalence and causes of visual impairment and blindness among 9980 Scandinavian adults: the Copenhagen City Eye Study. *Ophthalmology*. 2004;111:53–61.
6. Iwase A, Araie M, Tomidokoro A, Yamamoto T, Shimizu H, Kitazawa Y. Prevalence and causes of low vision and blindness in a Japanese adult population: the Tajimi Study. *Ophthalmology*. 2006;113:1354–1362.
7. Ohno-Matsui K, Shimada N, Yasuzumi K, et al. Long-term development of significant visual field defects in highly myopic eyes. *Am J Ophthalmol*. 2011;152:256–265.
8. Hayashi K, Ohno-Matsui K, Shimada N, et al. Long-term pattern of progression of myopic maculopathy: a natural history study. *Ophthalmology*. 2010;117:1595–1611.
9. Curtin BJ. Basic science and clinical management. In: Curtin BJ, ed. *The Myopias*. New York: Harper and Row; 1985:177–202.
10. Vongphanit J, Mitchell P, Wang JJ. Prevalence and progression of myopic retinopathy in an older population. *Ophthalmology*. 2002;109:704–711.
11. Moriyama M, Ohno-Matsui K, Hayashi K, et al. Topographical analyses of shape of eyes with pathologic myopia by high-resolution three dimensional magnetic resonance imaging. *Ophthalmology*. 2011;118:1626–1637.
12. Curtin BJ. The posterior staphyloma of pathologic myopia. *Trans Am Ophthalmol Soc*. 1977;75:67–86.
13. Hogan MJ. The sclera. In: Hogan ML, Alvarado JA, Weddle JE, eds. *Histology of the Human Eye*. Philadelphia, PA: W.B. Saunders; 1971:183–201.
14. Curtin BJ, Teng CC. Scleral changes in pathological myopia. *Trans Am Acad Ophthalmol Otolaryngol*. 1958;62:777–788.
15. Curtin BJ, Iwamoto T, Renaldo DP. Normal and staphylomatous sclera of high myopia. An electron microscopic study. *Arch Ophthalmol*. 1979;97:912–915.
16. McBrien NA, Gentle A. Role of the sclera in the development and pathological complications of myopia. *Prog Retin Eye Res*. 2003;22:307–338.
17. Avetisov ES, Savitskaya NF, Vinetskaya MI, Iomdina EN. A study of biochemical and biomechanical qualities of normal and myopic eye sclera in humans of different age groups. *Metab Pediatr Syst Ophthalmol*. 1983;7:183–188.
18. McBrien NA, Cornell LM, Gentle A. Structural and ultrastructural changes to the sclera in a mammalian model of high myopia. *Invest Ophthalmol Vis Sci*. 2001;42:2179–2187.
19. Rada JA, Shelton S, Norton TT. The sclera and myopia. *Exp Eye Res*. 2006;82:185–200.
20. Funata M, Tokoro T. Scleral change in experimentally myopic monkeys. *Graefes Arch Clin Exp Ophthalmol*. 1990;228:174–179.
21. Imamura Y, Iida T, Maruko I, Zweifel SA, Spaide RF. Enhanced depth imaging optical coherence tomography of the sclera in dome-shaped macula. *Am J Ophthalmol*. 2011;151:297–302.
22. Maruko I, Iida T, Sugano Y, Oyamada H, Sekiryu T. Morphologic choroidal and scleral changes at the macula in tilted disc syndrome with staphyloma using optical coherence tomography. *Invest Ophthalmol Vis Sci*. 2011;52:8763–8768.
23. Gaucher D, Erginay A, Lecleire-Collet A, et al. Dome-shaped macula in eyes with myopic posterior staphyloma. *Am J Ophthalmol*. 2008;145:909–914.
24. Yun SH, Bouma BE. Wavelength swept lasers. In: Drexler W, Fujimoto JG, eds. *Optical Coherence Tomography: Technology and Applications*. New York, NY: Springer; 2008:359–378.
25. Ohno-Matsui K, Akiba M, Moriyama M, Ishibashi T, Hirakata A, Tokoro T. Intrachoroidal cavitation in macular area of eyes with pathologic myopia. *Am J Ophthalmol*. In press.
26. Ohno-Matsui K, Akiba M, Moriyama M, Ishibashi T, Tokoro T, Spaide RF. Imaging the retrobulbar subarachnoid space around the optic nerve by swept source optical coherence tomography in eyes with pathologic myopia. *Invest Ophthalmol Vis Sci*. 2011;52:9644–9650.
27. Spaide RF, Akiba M, Ohno-Matsui K. Evaluation of peripapillary intrachoroidal cavitation with swept source and enhanced depth imaging optical coherence tomography. *Retina*. In press.
28. Ohno-Matsui K, Akiba M, Moriyama M, et al. Acquired optic nerve and peripapillary pits in pathologic myopia. *Ophthalmology*. In press.
29. Hsiang HW, Ohno-Matsui K, Shimada N, et al. Clinical characteristics of posterior staphyloma in eyes with pathologic myopia. *Am J Ophthalmol*. 2008;146:102–110.
30. Shauly Y, Miller B, Lichtig C, Modan M, Meyer E. Tenon's capsule: ultrastructure of collagen fibrils in normals and infantile esotropia. *Invest Ophthalmol Vis Sci*. 1992;33:651–656.
31. Fujiwara T, Imamura Y, Margolis R, Slakter JS, Spaide RF. Enhanced depth imaging optical coherence tomography of the choroid in highly myopic eyes. *Am J Ophthalmol*. 2009;148: 445–450.